Cooperative Slowdown of Water Rotation near Densely Charged Ions Is Intense but Short-Ranged

Ana Vila Verde[*,†,‡] and Reinhard Lipowsky[*,†]

Theory and Bio-Systems Department, Max Planck Institute of Colloids and Interfaces, Wissenschaftspark Golm, 14424 Potsdam, Germany;

E-mail: ana.vilaverde@mpikg.mpg.de; Reinhard.Lipowsky@mpikg.mpg.de

[*]To whom correspondence should be addressed

[†]Theory and Bio-Systems Department, Max Planck Institute of Colloids and Interfaces, Wissenschaftspark Golm, 14424 Potsdam, Germany;

[‡]Also at the University of Minho, Physics Center, Campus de Gualtar, 4710-057 Braga, Portugal.

Sulfate model

We develop parameters for the sulfate anion compatible with the SWM4-NDP water model, which explicitly includes polarizability using classical Drude oscillators. In the sulfate model developed and used in this work, only the oxygen atoms are polarizable. The sulfate model thus consists of nine interaction sites: the sulfur "S", four oxygens "O", and four Drude particles "D" each bonded to an oxygen site. All nine interaction sites have associated charge; the oxygen and sulfur sites have also associated Lennard-Jones potentials. The force-field used here has the form

$$U = k_{b,ij}(r_{ij} - r_{0,ij})^2 + k_{\theta,ijk}(\theta_{ijk} - \theta_{0,ijk})^2 + \epsilon_{ij}\left[\left(\frac{R_{min,ij}}{r_{ij}}\right)^{12} - 2\left(\frac{R_{min,ij}}{r_{ij}}\right)^{6}\right] + U_{electr} + U_{hyp} \tag{1}$$

The first term in Equation 1 is the bond potential: $r_{0,ij}$ is the equilibrium distance and r_{ij} the actual distance between bonded interaction sites i and j; $k_{b,ij}$ is the bond force constant. The second term is the angular potential: $\theta_{0,ijk}$ is the equilibrium angle and θ_{ijk} the actual angle formed by three consecutively bonded sites i, j and k; $k_{\theta,ijk}$ is the angular force constant. The third term is the typical Lennard-Jones potential used to mimic dispersive interactions between a pair of non-bonded sites i and j separated by distance r_{ij}, with the parameters $R_{min,ij}$ and ϵ_{ij} obtained from the self-interaction parameters as $R_{min,ij} = R_{min,ii}/2 + R_{min,jj}/2$ and $\epsilon_{ij} = \sqrt{\epsilon_{ii}\epsilon_{jj}}$. The fourth term, U_{electr}, encompasses the Coulomb interactions between pairs of charges in the system. Intramolecular electrostatic interactions between sulfate Drude pairs are calculated using the Thole screening function [1–3]:

$$U_{electr,Thole} = \frac{q_i q_j}{4\pi\varepsilon_0 r}\left[1 - \left(1 + \frac{r}{2a}\right)\exp(-r/a)\right] \tag{2}$$

where r is the distance between a pair of charges i and j, each belonging to a separate oxygen-Drude pair of the sulfate, $a = \sqrt[6]{\alpha_O^2}/t_{OO}$, α_O is the oxygen polarizability volume and t_{OO} is the dimensionless Thole screening parameter. All other intramolecular non-bonded

interactions in sulfate are excluded. Intermolecular Coulomb interactions are calculated in the usual manner for all pairs of charges. The fifth term, U_{hyp}, is an extra restoring force applied to the Drude-oxygen pair when the Drude spring is longer than r_{cut} to avoid polarization instabilities[2]: $U_{hyp} = k_{hyp}(r - r_{cut})^4$.

In addition to the U_{hyp}, the Drude-oxygen pairs interact also through the harmonic spring potential shown in Equation 1. This potential has spring constant $k_{b,OD}$ and equilibrium length $r_{0,OD} = 0$, so in the absence of an electric field and at non-zero temperature, the Drude particle oscillates around the core oxygen atom. In the presence of a field $\vec{E}$, force balance dictates that the average position of the Drude particle is displaced by $|q_D|E/(2k_{b,OD})$, with q_D the charge of the Drude particle associated with the oxygen atom. It follows that the average induced dipole is $q_D^2 E/(2k_{b,OD})$ and that the oxygen polarizability volume, α_O, is related to the value of $k_{b,OD}$ and the charge of the Drude particle as $q_D = -\sqrt{\alpha_O 8\pi\varepsilon_0 k_{b,OD}}$, with ε_0 the vacuum permittivity. We note that in the simulations performed here the Drude particle is at near-zero temperature, so the instantaneous electric field, $\vec{E}$, acting on the Drude particle can be straightforwardly obtained from the extension of the Drude spring at each time step:

$$\vec{E} = \begin{cases} \frac{2k_D\, r + 4k_{hyp}(r - r_{cut})^3}{q_D}\hat{r} & \text{, if } r \geq r_{cut} \\ \frac{2k_D\, r}{q_D}\hat{r} & \text{, if } r < r_{cut} \end{cases} \tag{3}$$

In this expression, $\vec{r} = r\hat{r}$ is the extension of the Drude spring, with $\hat{r}$ a unit vector.

All sulfate parameters are given in Table 1. The bonded parameters, masses, the charge and Lennard-Jones parameters for the sulfur and the total charge of the oxygen atom, equal to the sum of the charges of the oxygen and Drude sites ($q_O + q_D$), are from the references indicated. The parameters for non-bonded interactions involving the sulfate oxygen were obtained as described in the following section.

Table 1: Parameters for SO_4^{2-}.

Parameter	Value	Source
$k_{b,SO}$ (kcal/mol/Å^2)	500	[4]
$k_{b,OD}$ (kcal/mol/Å^2)	500	[2]
k_{hyp} (kcal/mol/Å^4)	40000	[2]
$r_{0,SO}$ (Å)	1.527	[4]
$r_{0,OD}$ (Å)	0	[2]
r_{cut} (Å)	0.2	[2]
$k_{\theta,OSO}$ (kcal/mole/rad^2)	141	[4]
$\theta_{0,OSO}$ (deg)	109.5	[4]
q_S ($\|e\|$)	+2	[4,5]
q_O ($\|e\|$)	+1.32823	This work
q_D ($\|e\|$)	-2.32823	This work
m_S (Da)	32.06	
m_O (Da)	15.5994	[2]
m_D (Da)	0.4	[2]
$R_{min,SS}/2$ (Å)	1.992370	[4,5]
$R_{min,OO}/2$ (Å)	1.950000	This work
ϵ_{SS} (kcal/mol)	0.25	[4,5]
ϵ_{OO} (kcal/mol)	0.15	This work
α_O (Å^3)	1.800000	This work
t_{OO}	2.6	[1]

Parameterization of sulfate

The Lennard-Jones parameters for the oxygen, $R_{min,OO}$, ϵ_{OO}, and the oxygen polarizability α_O are parameterized to reproduce three target properties – the minimum binding energy, E_{min}, and associated intermolecular distance, $r_{S\cdots O_W,min}$, of a complex with one sulfate ion and one water molecule (here termed sulfate monohydrate) from published ab initio calculations, and the difference in hydration free energy, $\Delta\Delta G^{hydr}$, at infinite dilution between Cl^- and SO_4^{2-}– while meeting the condition that the total sulfate polarizability remains within physically reasonable bounds. Our results show that all these conditions cannot be simultaneously satisfied by any combination of the oxygen parameters. Because differences in hydration free energies are expected to have lower uncertainty than results from ab initio simulations, the final set of parameters is chosen to accurately reproduce $\Delta\Delta G^{hydr}$ while keeping the difference between the calculated and the target values of the other two proper-

ties below 10%.

Calculating monohydrate properties

We perform simulations of sulfate monohydrate in the bidentate configuration shown in Figure 1, where each water hydrogen interacts with one sulfate oxygen and the water dipole is in the plane defined by the coordinated sulfate oxygens and the sulfur. The calculations are performed with sulfate and water in their equilibrium isolated geometries; only the Drude particles are allowed to move. This configuration was selected because its minimum energy, E_{min}, and associated distance between the sulfur and the water oxygen, $r_{S\cdots O_w,min}$, are known from ab initio calculations[5]. The values of the target properties are shown in Table 2.

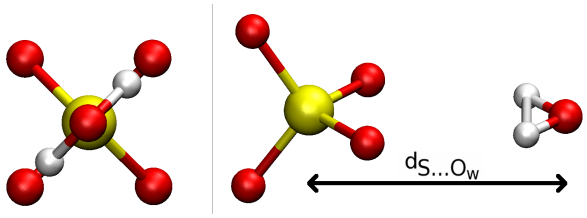

(a) (b)

Figure 1: (a) Top- and (b) side-view of simulated monohydrate configuration.

Table 2: Target values of the properties used to parameterize sulfate, and values calculated using the parameterized model. The source of each reference value is given in brackets. E_{min} is the minimum binding energy of the sulfate monohydrate with the configuration shown in Figure 1 , $r_{S\cdots O_W,min}$ is the distance between the sulfur and the water oxygen at the minimum energy configuration, $\Delta\Delta G^{hydr} = \Delta G^{hydr}_{SO_4^{2-}} - \Delta G^{hydr}_{Cl^-}$ is the difference in the standard free energy of hydration of Cl^- and SO_4^{2-}.

Quantity	Target value	Parameterized model
$r_{S\cdots O_W,min}$ (Å); [5]	3.44	3.47
E_{min} (kcal/mol); [5]	-25.65	-23.84
$\Delta\Delta G^{hydr}$ (kcal/mol); [6]	-177.58	-177.42
$\alpha_{SO_4^{2-}}$ (Å^3); [4,7,8]	5.56; 7.1; 9.43	7.2

We test all possible combinations of the oxygen Lennard-Jones parameters ϵ_{OO} =0.10, 0.15, 0.20, 0.25 and 0.30 kcal/mol, $R_{min,OO}/2$=1.70, 1.75, 1.80, 1.85, 1.90, 1.95 and 2.0 Å and

the oxygen polarizability volume α_O =1.4, 1.6, 1.8, 2.0 and 2.2 Å^3. The range of Lennard-Jones parameter values is chosen to bracket those from non-polarizable models of SO_4^{2-}; the range for the polarizability volume encompasses known values for sulfate, as shown in Table 2. For each parameter combination, we calculate the system energy, E, as a function of the distance, r, between the sulfur and the water oxygen (O_w) and obtain the minimum energy E_{min} and associated $r_{S\cdots O_w,min}$.

Simulations are performed using NAMD. The $S\cdots O_w$ separation is varied between 3 and 6 Å in 0.01 Å increments, and each $S\cdots O_w$ configuration is simulated for 100000 steps. Electrostatic and Lennard-Jones interactions are calculated using an infinite cutoff. The equations of motion are integrated every 0.2 fs. The SETTLE algorithm is used to fix the geometry of the non-Drude particles[9]. Classical dynamic trajectories near the self-consistent field limit are generated by using extended Lagrangian dynamics with a dual-Langevin thermostat[3]. The target temperature for the Drude thermostat is 0.1 K and for the remaining degrees of freedom 1 K, with a damping coefficient of 5 ps^{-1} used in both thermostats.

Calculating free energies of hydration

We calculate the free energy of hydration of sulfate using Free Energy Perturbation as implemented in NAMD. This calculation is done in two stages. In the first stage, approximate free energies, with an estimated uncertainty of ±2 kcal/mol, are calculated using short simulation times for all possible combinations of the oxygen Lennard-Jones parameters ϵ_{OO} =0.10, 0.15, 0.175, 0.20, 0.225 and 0.25 kcal/mol, $R_{min,OO}/2$=1.70, 1.75, 1.80, 1.85, 1.90 and 1.95 Å and the oxygen polarizability volume α_O =1.4, 1.6, 1.8, 2.0 and 2.2 Å^3. The free energies obtained this way are used in conjunction with the results of the monohydrate simulations to identify the narrow region of $R_{min,OO}/2$, ϵ_{OO} and α_O parameter values that better reproduce the target properties, as described below. In the second stage, accurate values of the free energy of hydration are then calculated for a reduced number of the most promising parameter

sets using longer simulation times so that the best oxygen parameters can be identified.

The simulation box consists of one sulfate ion and 823 water molecules and has approximate dimensions $29.1 \times 29.1 \times 29.1$ Å^3. Periodic boundary conditions are used. Electrostatic interactions are calculated directly up to 12 Å and using Particle Mesh Ewald with a 1 Å grid spacing, 4^{th} order interpolation and 10^{-6} tolerance for larger particle separations. Van der Waals interactions are smoothly switched to zero between 10 and 12 Å. Energy and pressure corrections are not used. Simulations are performed in the NPT ensemble. The target temperature for the Drude thermostat is 1 K and for the remaining degrees of freedom 298.15 K, with a damping coefficient of 5 ps^{-1} used in both thermostats. The constant pressure requirement is satisfied by using a Langevin barostat with a target pressure 1 atm, oscillation period 100 fs and damping timescale 100 fs. Full electrostatic interactions are evaluated every 2 fs, and all other interactions every 1 fs.

For each parameter combination, the free energy of hydration is calculated by integrating along an artificial path between an isolated sulfate ion+isolated water box and a fully solvated ion in a water box with the same number of water molecules. This path is characterized by a path coordinate, λ.[1] For accurate integration, the path is split into two processes: Lennard-Jones interactions between the ion and the water are smoothly switched on as λ varies between 0 and 0.5 while the same is done for the electrostatic interactions as λ varies between 0.5 and 1. In addition, the Lennard-Jones interactions between the ion and the water are kept finite for all values of λ by using a soft-core van der Waals radius-shifting coefficient of 5 Å. The integration path is broken into many windows, each of which is characterized by two consecutive values of the path coordinate. For each window, we perform forward and backward transformations and calculate a partial free energy using Bennett's acceptance ratio[10]. The free energy calculations performed during the first stage mentioned above use

[1] λ assumes the values 0 0.025 0.05 0.075 0.1 0.125 0.15 0.175 0.2 0.225 0.25 0.275 0.3 0.325 0.35 0.375 0.4 0.425 0.45 0.475 0.5 0.525 0.55 0.575 0.6 0.62 0.64 0.655 0.67 0.68 0.69 0.7 0.71 0.72 0.73 0.74 0.75 0.755 0.76 0.765 0.77 0.775 0.78 0.785 0.79 0.795 0.8 0.805 0.81 0.815 0.82 0.825 0.83 0.835 0.84 0.845 0.85 0.855 0.86 0.865 0.87 0.875 0.88 0.885 0.89 0.895 0.9 0.905 0.91 0.915 0.92 0.925 0.93 0.935 0.94 0.945 0.95 0.955 0.96 0.965 0.97 0.975 0.98 0.985 0.99 0.995 1

400 equilibration and 3600 production steps for each window; the final free energy estimates, obtained during the second stage, use 400000 equilibration and 800000 production steps. Simulations using this number of steps per window yield the same free energy of hydration as simulations using 10000 equilibration and 40000 production steps per window, indicating that the calculated free energies are reliable. The total hydration free energy from the simulation is obtained by summing over all the partial free energies along the path.

Correction terms to the free energy

The free energy of hydration calculated directly from the simulation, ΔG_{sim}^{hydr}, must be corrected before it can be compared with experiment[11,12]. We apply the same correction terms used to develop the other ion models used in these simulations[2].

(i) Correction of the dependence of the calculated value on the size of the simulation box. A dependence of the free energy on the box size arises when electrostatic interactions are calculated using Ewald sums because of interactions between the periodic images[13]. The largest of these interactions is that associated with the disappearance of the isolated ion: at $\lambda = 0$, the free energy calculated directly from the simulation includes a positive contribution from the interaction of the isolated ion with its periodic images and the homogeneous neutralizing background charge density; at $\lambda = 1$, this contribution is no longer present. For a cubic simulation box with length L as those used here, this Wigner correction term is

$$\Delta G_{PME} = -\frac{|e|^2}{8\pi\varepsilon_0}(z_f^2 - z_i^2)\left(\frac{-2.837297}{L}\right) \tag{4}$$

where z_i and z_f are the charge numbers at the beginning and the end, i.e. at $\lambda = 0$ and $\lambda = 1$, of a FEP simulation. For the isolated ion, $z_i = -2$ and $z_f = 0$. Smaller correction terms, accounting for the appearance of self-interactions between the periodic images of the solvated ion and the orientation polarization of the solvent, could also be applied[11–13]. We do not do so here to remain consistent with the procedure used to parameterize the other

ions used in this study[2].

(ii) Correction for the change of concentration of the ion between the vapor and aqueous phases. Experimental free energies of hydration are reported for standard states for the vapor and aqueous phases, i.e., an ideal gas at 1 atm for the vapor phase and an ideal aqueous solution at 1 M concentration. Because in the simulations the vapor and aqueous phases have the same volume, the free energy value calculated directly from the simulation lacks the entropic contribution associated to the change in volume between the vapor and aqueous standard states. This entropic contribution, ΔG_{press}, is

$$\Delta G_{press} = -T\Delta S_{press} = -k_B T \ln\left(\frac{V_l}{V_g}\right) \tag{5}$$

where $V_l = 1$ l/mol is the molar volume of an ideal aqueous solution of concentration 1 M and $V_g = 24.465$ l/mol is that of an ideal gas at 1 atm.

(iii) Correction for the potential drop when crossing the air-water interface. Published free energies of hydration of isolated ions include an estimated contribution from the potential drop associated with the air-water interface. Because this interface does not exist in the simulations, the free energy value obtained directly from the simulation lacks this term. The free energy correction, ΔG_{surf}, is given by

$$\Delta G_{surf} = z|e|V_{surf} \tag{6}$$

where V_{surf} is the surface potential. We use $V_{surf} = -0.545$ V, the same value that was used to develop[2] the ion parameters for Cs^+, $Cl^-$and Mg^{2+}; for SO_4^{2-}, $z = -2$.

The free energy of hydration of an ion, ΔG^{hydr}, can be calculated by adding the correction terms to the value directly calculated from the simulation, ΔG^{hydr}_{sim}:

$$\Delta G^{hydr} = \Delta G^{hydr}_{sim} + \Delta G_{PME} + \Delta G_{press} + \Delta G_{surf} \tag{7}$$

The values of the various correction terms for the free energy of hydration of sulfate, as well as the final value of the free energy of hydration calculated using the optimum parameters are given in Table 3. For comparison, the same quantities are given for Cl^-.

Table 3: Free energy of hydration of sulfate and chloride, and their various contributions, in kcal/mol. ΔG_{sim}^{hydr} is the value directly calculated from the simulation using the optimum parameters; ΔG^{hydr} is the value including all the correction terms, which can be compared directly to the published values obtained from experiment.

ion	ΔG_{sim}^{hydr}	ΔG_{PME}	ΔG_{press}	ΔG_{surf}	ΔG^{hydr}
SO_4^{2-}	-218.31	-64.6	1.888	25.2	-255.8
Cl^-	-76.7	-16.15	1.888	12.6	-78.4

Optimization procedure

For each value of $R_{min,OO}/2$ tested, the E_{min}, $r_{S\cdots O_w,min}$ and $\Delta\Delta G^{hydr}$ surfaces are fitted with the following functions of ϵ_{OO} and α_O:

$$E_{min} = e_0 + e_1\epsilon_{OO} + e_2\alpha_O \tag{8}$$

$$r_{S\cdots O_w,min} = d_0 + d_1\epsilon_{OO} + d_2\alpha_O \tag{9}$$

and

$$\Delta\Delta G^{hydr} = h_0 + h_1\epsilon_{OO} + h_2\alpha_O \tag{10}$$

where e_i, d_i and h_i ($i = 0, 1, 2$) are fitting parameters. Equations 8, 9 and 10 are then equated to the target E_{min}, $r_{S\cdots O_W,min}$ and $\Delta\Delta G^{hydr}$ (shown in Table 2) to obtain the ϵ_{OO} and α_O combinations that, at each $R_{min,OO}/2$, reproduce the target data. The three curves obtained for each $R_{min,OO}/2$ (not shown) do not intersect, and the trends indicate that it is impossible to obtain a set of parameters that simultaneously reproduces all target properties. Because the free energies of hydration are expected to have lower uncertainty than the monohydrate values, we focus on a narrow region of parameter space that reproduces the $\Delta\Delta G^{hydr}$ while

keeping the difference between the target and the calculated monohydrate properties below 10%. For the reduced number of parameter sets in this region ($R_{min,OO}/2 = 1.95$ Å, $\epsilon_{OO} = -0.15$ kcal/mol, $\alpha_O = 1.6, 1.8, 2.0$ Å^3), we recalculate $\Delta\Delta G^{hydr}$ using long simulations. We find that the parameter set shown in Table 1 reproduces the experimental $\Delta\Delta G^{hydr}$ while leading to values of E_{min} within 7% and $r_{S\cdots O_w,min}$ within 1% of the target values. We note that equally good agreement between the calculated and the target properties could be obtained for slightly different sets of parameters, indicating that it is possible to further improve the sulfate model by parameterizing it against other target properties such as solvation entropies. We opted not to do so here to remain consistent with the parameterization procedure used to obtain the parameters of the other ions.

Ion-O_w radial distribution functions

The radial distribution functions of the water oxygen relative to the each of the four ions are shown in Figure 2. The position and height of the S-O_w extrema for SO_4^{2-} are shown in Table 4. These values are obtained by fitting each minimum or maximum with a Gaussian function $a\exp(\pm\frac{(x-\mu)^2}{2c^2})$: the position of each peak is given by μ and its height by a.

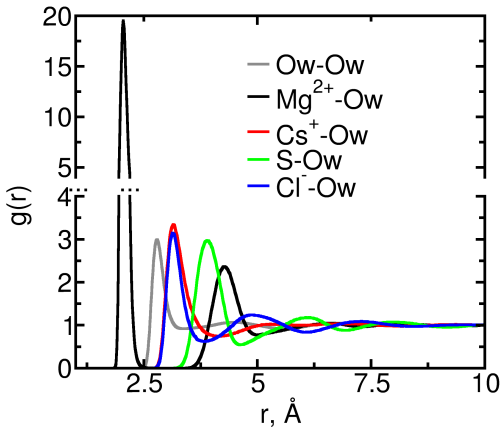

Figure 2: Ion-water oxygen (O_w) radial distribution functions. For comparison the O_w-O_w radial distribution function is also shown. The radial distribution function for the sulfate anion is calculated relative to the sulfur.

Table 4: Position (r, Å) and intensity (g) of the minima and maxima of the sulfur-water oxygen radial distribution function.

Quantity	Value
$r_{max,1}$	3.899
$g_{max,1}$	2.978
$r_{min,1}$	4.639
$g_{min,1}$	0.536
$r_{max,2}$	6.084
$g_{max,2}$	1.174
$r_{min,2}$	6.948
$g_{min,2}$	0.880
$r_{max,3}$	7.993
$g_{max,3}$	1.072
$r_{min,3}$	9.175
$g_{min,3}$	0.952

Residence times of water near isolated ions

The residence times of water in each of the hydration shells of the ions are calculated using the stable states picture model proposed by Northrup and Hynes[14], as implemented by Joung and Cheatham[15]. In this approach, water molecules that only leave the hydration shell very briefly are not considered in the calculation of the residence time; only stable transitions to the neighboring hydration shells are considered. To identify these transitions we define *stable* reactant (R) and product (P) states from the positions of the minima and maxima of the ion-O_w radial distribution function. The upper (or right hand side) boundary of the reactant state associated with peak i of the radial distribution function is the radius satisfying $g(r_R) = \sqrt{g(r_{max,i})g(r_{min,i})}$; the lower boundary of the right hand side product state is that satisfying $g(r_P) = \sqrt{g(r_{min,i})g(r_{max,i+1})}$. Analogous expressions are used to define the left hand side boundaries of the reactant and product states, if they exist. Using these definitions of stable reactant and product states and absorbing boundary conditions in the product, we calculate the probability, $p(t)$, that a molecule in the reactant state at $t = 0$ will be in the product state at time t. The probability curves are well fitted by the function $1 - \exp(-t/\tau_{res})$, from which the residence times, τ_{res}, are obtained. The residence times of water in the hydration shells of each of the four ions are shown in Table 5.

Table 5: Residence times of water molecules in the hydration shells of the ions. The residence time for water molecules in the first hydration shell of Mg^{2+} could not be calculated because no transitions occurred in our simulations.

ion	hydration shell	τ_{res} (ps)
Mg^{2+}	1	–
Mg^{2+}	2	16.7
Cs^{+}	1	8.8
Cs^{+}	2	6.2
SO_4^{2-}	1	23.0
SO_4^{2-}	2	9.4
Cl^{-}	1	11.9
Cl^{-}	2	8.9

Reorientation of water in the bulk and near isolated ions

We characterize the reorientation of the OH groups and water dipoles for different water subpopulations near isolated cations and anions. We distinguish these subpopulations by their initial distance relative to the anion or the cation: at $t = 0$ of the reorientation autocorrelation functions, the oxygens of each water subpopulation must belong to a hollow sphere of radius d and thickness 1 Å centered around the ion.

Our results indicate that Mg^{2+}, SO_4^{2-} and Cl^- strongly slowdown the reorientation of water in their first hydration layer ($d = 2$ Å for Mg^{2+}, $d = 4$ Å for SO_4^{2-}, $d = 3$ Å for Cl^-). The effect of Cl^- and SO_4^{2-} ions on water rotation does not extend beyond their second hydration layer ($d = 5$ Å for Cl^-, $d = 6$ Å for SO_4^{2-}), but are still present in the third hydration layer of Mg^{2+} ($d = 6$ Å). For all three ions, however, the magnitude of the slowdown in these external hydration layers is much smaller than that found for the first hydration layer. The effect of Cs^+ on water reorientation contrasts markedly to that found for the other three ions, with all water subpopulations near Cs^+ displaying reorientation dynamics similar to water in the bulk.

It has been previously suggested that cations and anions have a strongly anisotropic effect on water dynamics, with cations affecting the reorientation of hydroxyl groups and anions affecting the reorientation of the water dipoles[16,17]. Our results do not support this scenario; rather, the anisotropic effect of cations and anions on water dynamics is weak: the effect of all four ions on the reorientation of OH groups is comparable to their effect on the reorientation of dipoles.

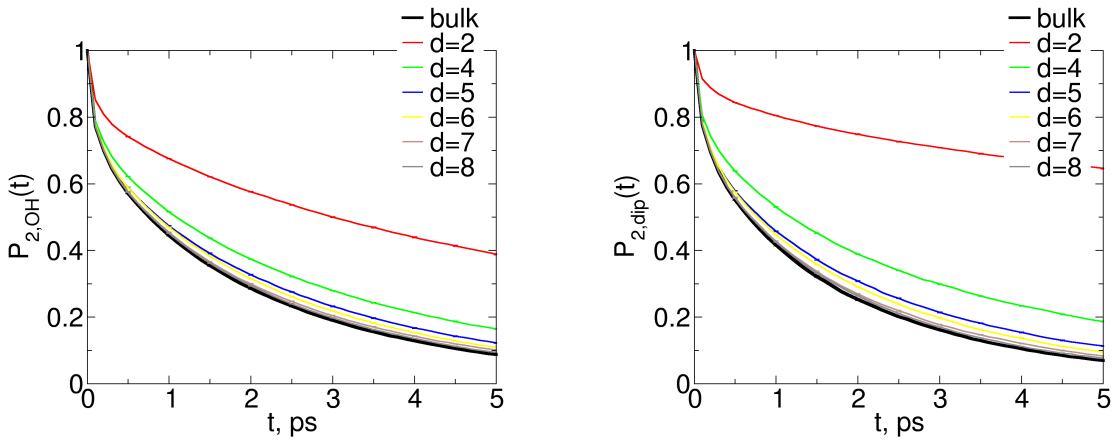

(a) (b)

Figure 3: Reorientation decay for different water subpopulations around an isolated Mg^{2+} ion. $P_2(t)$ is calculated for (a) water OH groups and (b) water dipoles, for water molecules with their oxygen atom within a hollow sphere of radius d and thickness 1 Å centered on Mg^{2+} at $t = 0$. To facilitate comparisons, each panel also shows the relevant decay curve for water in the bulk.

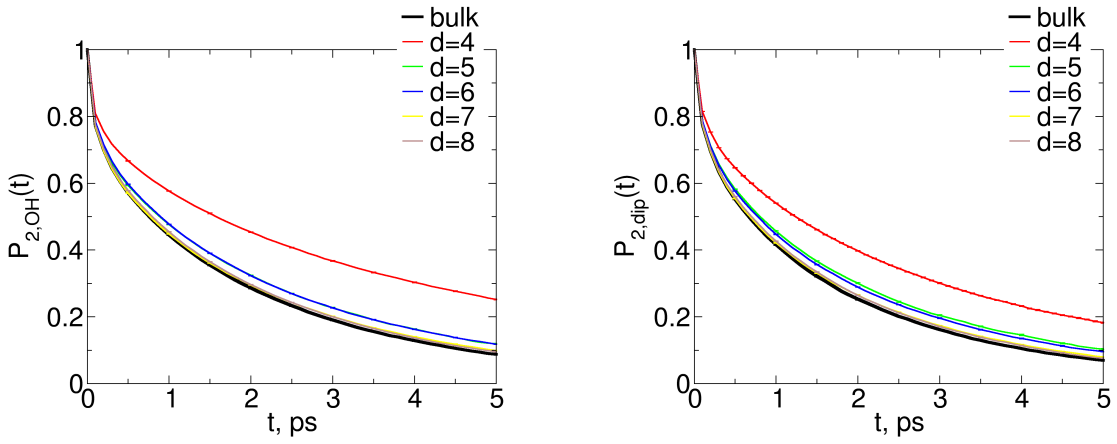

(a) (b)

Figure 4: Reorientation decay for different water subpopulations around an isolated SO_4^{2-} ion. $P_2(t)$ is calculated for (a) water OH groups and (b) water dipoles, for water molecules with their oxygen atom within a hollow sphere of radius d and thickness 1 Å centered on SO_4^{2-} at $t = 0$. To facilitate comparisons, each panel also shows the relevant decay curve for water in the bulk.

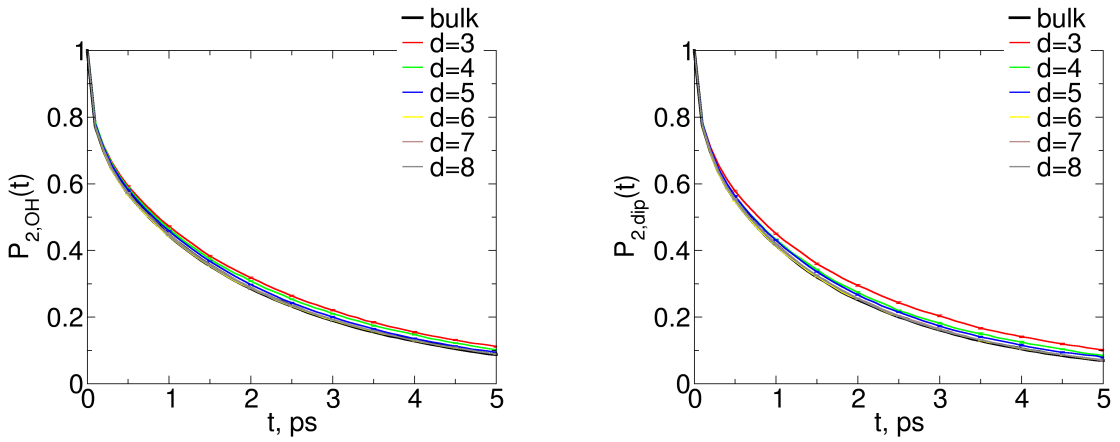

(a) (b)

Figure 5: Reorientation decay for different water subpopulations around an isolated Cs^+ ion. $P_2(t)$ is calculated for (a) water OH groups and (b) water dipoles, for water molecules with their oxygen atom within a hollow sphere of radius d and thickness 1 Å centered on Cs^+ at $t = 0$. To facilitate comparisons, each panel also shows the relevant decay curve for water in the bulk.

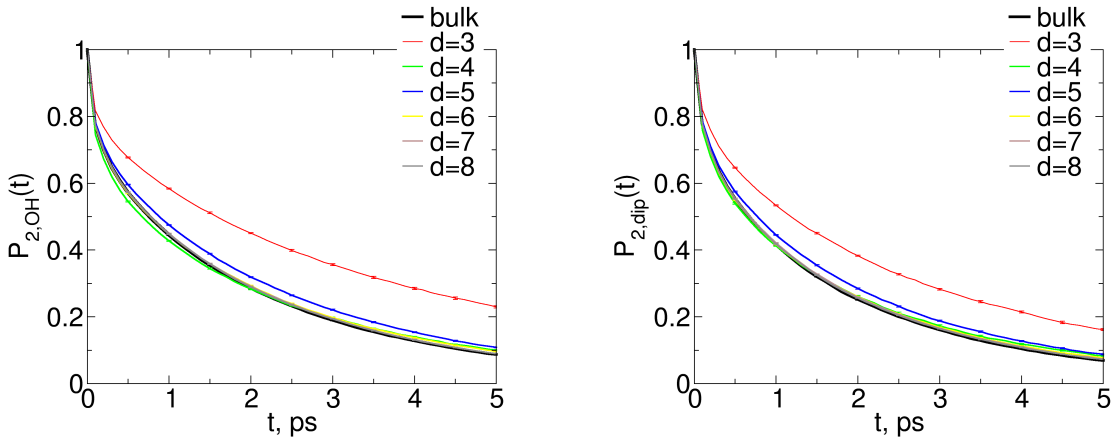

(a) (b)

Figure 6: Reorientation decay for different water subpopulations around an isolated Cl^- ion. $P_2(t)$ is calculated for (a) water OH groups and (b) water dipoles, for water molecules with their oxygen atom within a hollow sphere of radius d and thickness 1 Å centered on Cl^- at $t = 0$. To facilitate comparisons, each panel also shows the relevant decay curve for water in the bulk.

As described in the main text, the $P_{2,x}(t)$ curves obtained for each water subpopulation in the systems with isolated ions were fitted, for $t < 20$ ps, by a sum of three exponentials. The

average time constants characteristic of OH or dipole reorientation, $\tau_{isol,x}$, were then obtained from the fitting parameters as the weighted sum of the three time constants extracted from the fit. These time constants are shown in Table 6. For comparison, the same table shows τ_{OH} and τ_{dip} for water in the bulk, calculated using the same procedure.

Table 6: Average time constants characteristic of OH ($\tau_{isol,OH}$) and dipole ($\tau_{isol,dip}$) reorientation for different water subpopulations near isolated ions. For comparison the average time constants for water in the bulk are also given.

Ion	Water subpopulation(d,Å)	$\tau_{isol,OH}$ (ps)	$\tau_{isol,dip}$ (ps)
–	Bulk	1.69	1.50
Cs^+	3	1.94	1.85
Cs^+	4	1.85	1.66
Cs^+	5	1.77	1.61
Cs^+	6	1.69	1.53
Cs^+	7	1.70	1.52
Cs^+	8	1.70	1.52
Cl^-	3	3.38	2.56
Cl^-	4	1.79	1.60
Cl^-	5	1.93	1.70
Cl^-	6	1.77	1.57
Cl^-	7	1.72	1.55
Cl^-	8	1.71	1.54
Mg^{2+}	2	6.45	23.7
Mg^{2+}	4	2.52	3.07
Mg^{2+}	5	2.07	1.99
Mg^{2+}	6	1.92	1.80
Mg^{2+}	7	1.81	1.65
Mg^{2+}	8	1.75	1.58
SO_4^{2-}	3	3.37	2.78
SO_4^{2-}	4	3.91	2.80
SO_4^{2-}	5	2.01	1.91
SO_4^{2-}	6	2.01	1.80
SO_4^{2-}	7	1.80	1.61
SO_4^{2-}	8	1.77	1.59

Cooperative slowdown factors of water subpopulations near individual pairs of ions

The cooperative slowdown factors for the various configurations of magnesium sulfate and cesium chloride investigated here are shown in Figures 7 ,8, 9 and 10. For each subpopulation, the values of the average time constants characterizing the reorientation of OH groups or water dipoles can be obtained by multiplying the cooperative slowdown factors by the time constant, $\tau_{isol,x}$, characterizing the reorientation of the water subpopulation at the same distance d from the isolated ion (see Table 6).

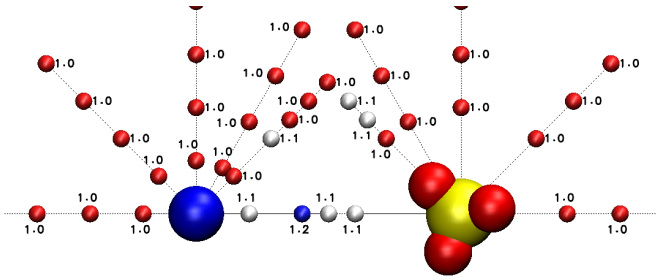

(a) $D = 10$ Å.

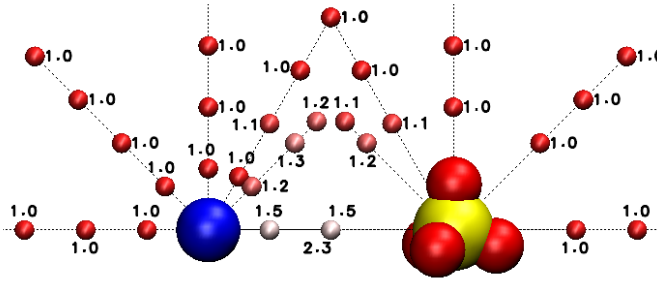

(b) $D = 8$ Å.

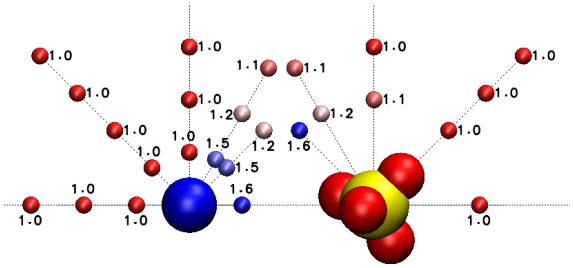

(c) $D = 7$ Å.

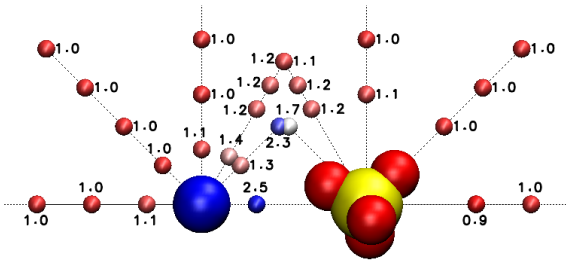

(d) $D = 6$ Å.

Figure 7: Cooperative slowdown factor, f_c, associated with the reorientation of OH groups of water subpopulations that at $t = 0$ are at the indicated positions relative to the Mg^{2+} (large blue sphere) and SO_4^{2-} (red and yellow spheres) ions, for various anion-cation separations D. The color scale of the smaller spheres conveys, for each panel, the magnitude of the cooperative slowdown factor shown next to the spheres. Consecutive water subpopulations along the dashed lines are 1 or 2 Å apart.

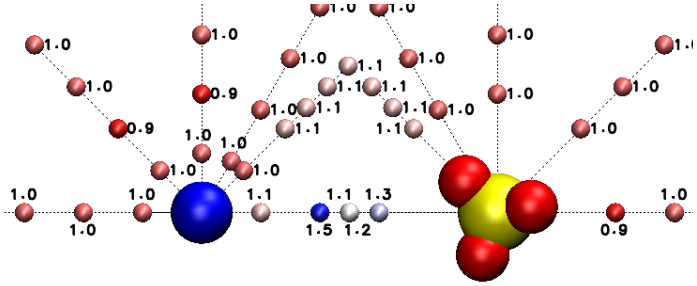

(a) $D = 10$ Å.

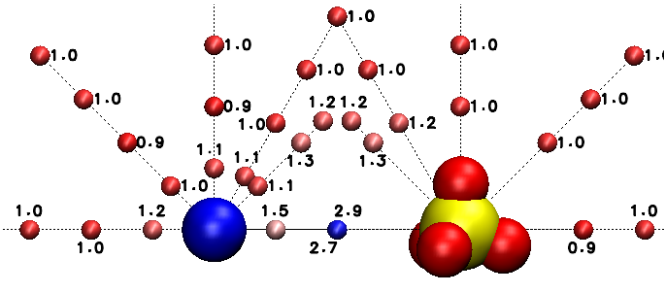

(b) $D = 8$ Å.

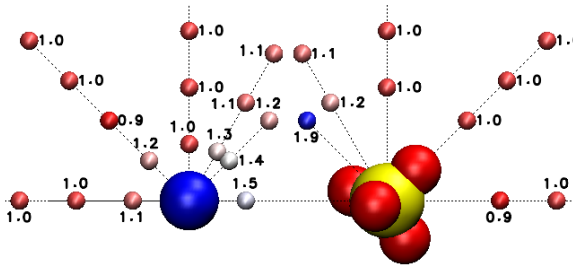

(c) $D = 7$ Å.

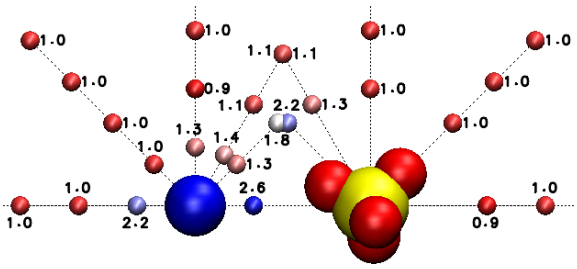

(d) $D = 6$ Å.

Figure 8: Cooperative slowdown factor, f_c, associated with the reorientation of water dipoles of subpopulations that at $t = 0$ are at the indicated positions relative to the Mg^{2+} (large blue sphere) and SO_4^{2-} (red and yellow spheres) ions, for various anion-cation separations D. The color scale of the smaller spheres conveys, for each panel, the magnitude of the cooperative slowdown factor shown next to the spheres. The subpopulations closest to Mg^{2+} are at $d = 2$ Å and those closest to SO_4^{2-} at $d = 4$ Å. Consecutive water subpopulations along the dashed lines are 1 or 2 Å apart.

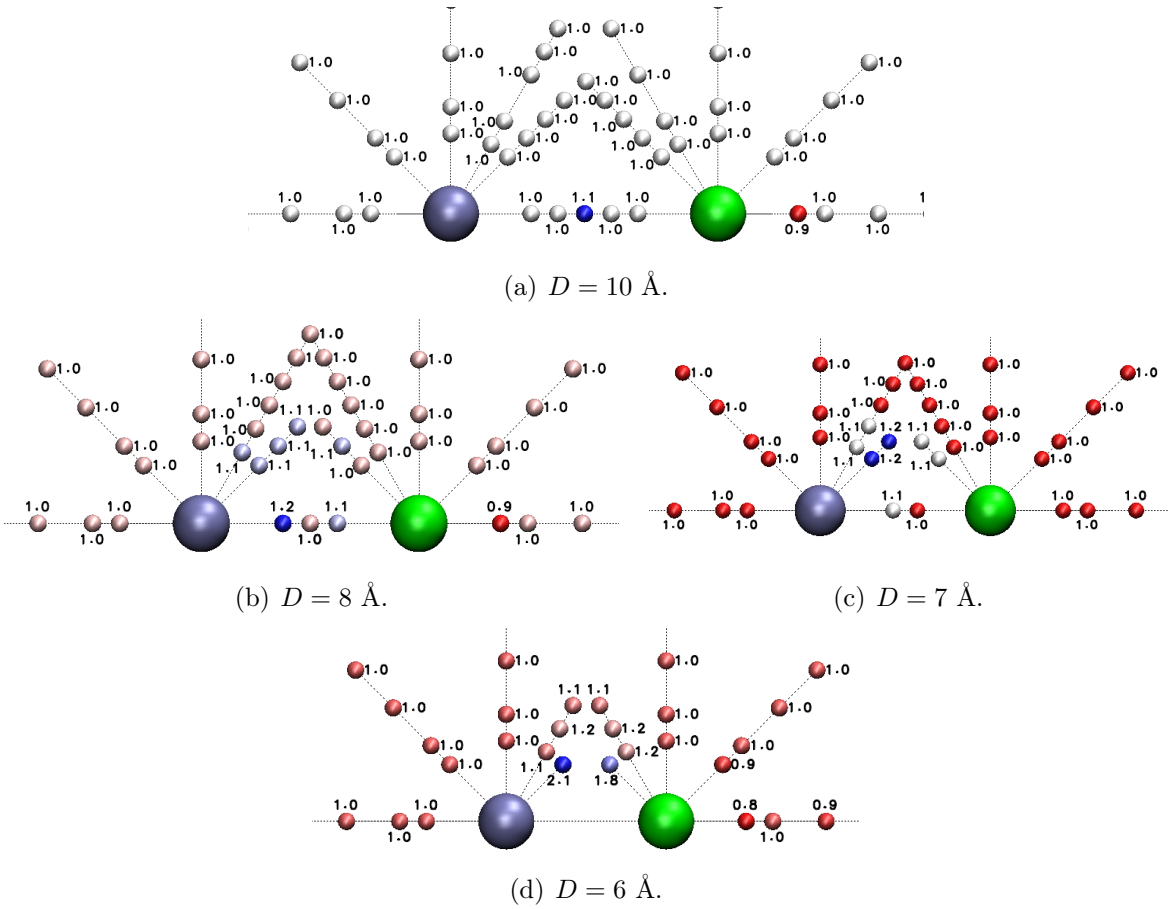

(a) $D = 10$ Å.

(b) $D = 8$ Å.

(c) $D = 7$ Å.

(d) $D = 6$ Å.

Figure 9: Cooperative slowdown factor, f_c, associated with the reorientation of OH groups of water subpopulations that at $t = 0$ are at the indicated positions relative to the Cs^+ (large light blue sphere) and Cl^- (green sphere) ions, for various anion-cation separations D. The color scale of the smaller spheres conveys, for each panel, the magnitude of the cooperative slowdown factor shown next to the spheres. The subpopulations closest to either ion are at $d = 3$ Å. Consecutive water subpopulations along the dashed lines are 1 or 2 Å apart.

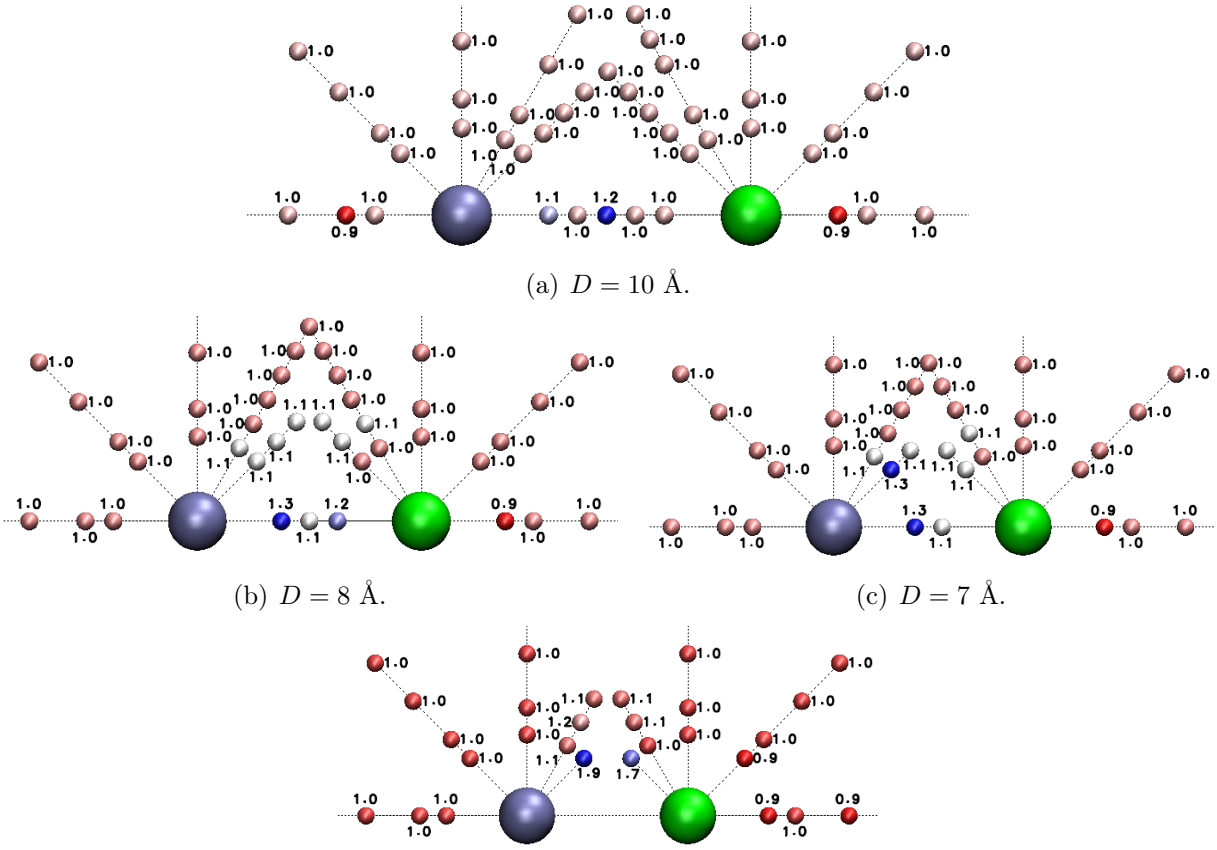

(a) $D = 10$ Å.

(b) $D = 8$ Å.

(c) $D = 7$ Å.

(d) $D = 6$ Å.

Figure 10: Cooperative slowdown factor, f_c, associated with the reorientation of water dipoles of subpopulations that at $t = 0$ are at the indicated positions relative to the Cs^+ (large light blue sphere) and Cl^- (green sphere) ions, for various anion-cation separations D. The color scale of the smaller spheres conveys, for each panel, the magnitude of the cooperative slowdown factor shown next to the spheres. The subpopulations closest to either ion are at $d = 3$ Å. Consecutive water subpopulations along the dashed lines are 1 or 2 Å apart.

Correlation between cooperative slowdown factors and changes in the electric field near individual ion pairs

We investigate whether cooperative slowdown of water rotation by individual ion pairs correlates with differences between the electric field in systems with ion pairs and in those with individual ions only. The average electric field on each water molecule can be obtained directly from the simulations from the extension of the Drude bond of the water molecules, as described in page 2. We calculate the average electric field (E) acting on each (ion, d, θ) subpopulation in the systems with ion pairs and on the corresponding subpopulation at the same d near the isolated ion (E_{isol}). If cooperative slowdown near ion pairs, relative to isolated ions, results from differences in the electric field between these two systems, we expect the cooperative slowdown factors to correlate with the ratio E/E_{isol}. In Figure 11 we show the cooperative slowdown factors as a function of the ration E/E_{isol}. These results indicate, as described in the main text, that the weak cooperative slowdown of water by Mg^{2+}-SO_4^{2-} pairs at large anion-cation separation correlates with the appearance of slightly more intense electric fields halfway between the ions, suggesting that changes in the electric field are at the origin of the observed cooperative slowdown. In contrast, the strong cooperative slowdown observed for the shortest anion-cation separations does not correlate with changes in the electric field.

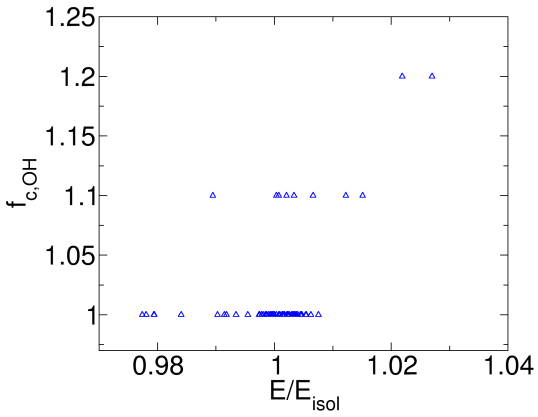

(a) $D = 10, 12$ Å.

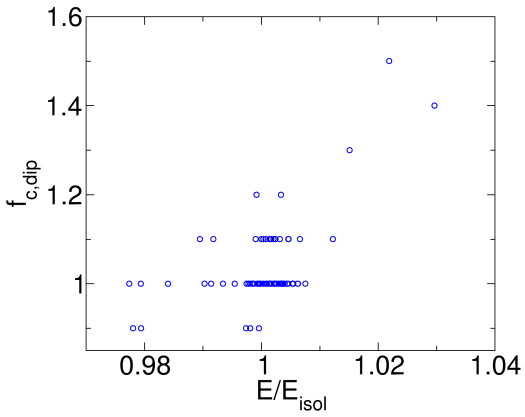

(b) $D = 10, 12$ Å.

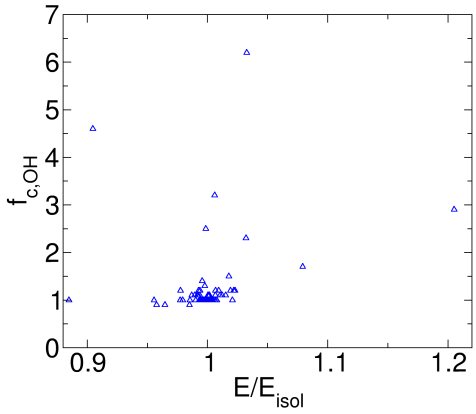

(c) $D = 5, 6$ Å.

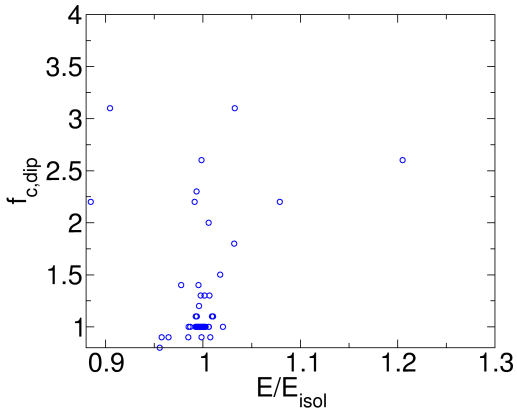

(d) $D = 5, 6$ Å.

Figure 11: Cooperative slowdown factors, $f_{c,x}$, for different water subpopulations near individual Mg^{2+}-SO_4^{2-} as a function of the ratio of the electric field experienced by those subpopulations to the electric field of the corresponding subpopulation near isolated ions, E/E_{isol}. The plots show data for all subpopulations in systems with small ($D = 5, 6$ Å) or large ($D = 10, 12$ Å) Mg^{2+}-SO_4^{2-} separation.

References

(1) Harder, E.; Anisimov, V. M.; Whitfield, T.; MacKerell, A. D.; Roux, B. Understanding the Dielectric Properties of Liquid Amides from a Polarizable Force Field. *J. Phys. Chem. B* **2008**, *112*, 3509–3521.

(2) Yu, H.; Whitfield, T. W.; Harder, E.; Lamoureux, G.; Vorobyov, I.; Anisimov, V. M.; MacKerell, J., Alexander D.; Roux, B. Simulating Monovalent and Divalent Ions in Aqueous Solution Using a Drude Polarizable Force Field. *J. Chem. Theory Comput.* **2010**, *6*, 774–786.

(3) Jiang, W.; Hardy, D. J.; Phillips, J. C.; MacKerell, A. D.; Schulten, K.; Roux, B. High-Performance Scalable Molecular Dynamics Simulations of a Polarizable Force Field Based on Classical Drude Oscillators in NAMD. *J. Phys. Chem. Lett.* **2010**, *2*, 87–92.

(4) Ishiyama, T.; Morita, A. Molecular Dynamics Simulation of Sum Frequency Generation Spectra of Aqueous Sulfuric Acid Solution. *J. Phys. Chem. C* **2011**, *115*, 13704–13716.

(5) Cannon, W. R.; Pettitt, B. M.; McCammon, J. A. Sulfate Anion in Water: Model Structural, Thermodynamic, and Dynamic Properties. *J. Phys. Chem.* **1994**, *98*, 6225–6230.

(6) Marcus, Y. *Ion Properties*; Marcel Dekker, Inc.: New York, USA, 1997.

(7) Jungwirth, P.; Curtis, J. E.; Tobias, D. J. Polarizability and Aqueous Solvation of the Sulfate Dianion. *Chem. Phys. Lett.* **2003**, *367*, 704–710.

(8) Serr, A.; Netz, R. R. Polarizabilities of Hydrated and free Ions derived from DFT Calculations. *Int. J. Quantum Chem.* **2006**, *106*, 2960–2974.

(9) Miyamoto, S.; Kollman, P. A. Settle: An Analytical Version of the SHAKE and RATTLE Algorithm for Rigid Water Models. *J. Comput. Chem.* **1992**, *13*, 952–962.

(10) Chipot, C., Pohorille, A., Eds. *Free Energy Calculations - Theory and Applications in Chemistry and Biology*; Springer Series in chemical physics; Springer Berlin / Heidelberg, 2007; Vol. 86.

(11) Horinek, D.; Mamatkulov, S. I.; Netz, R. R. Rational design of Ion Force Fields based on thermodynamic Solvation Properties. *J. Chem. Phys.* **2009**, *130*, 124507.

(12) Warren, G. L.; Patel, S. Hydration Free Energies of Monovalent Ions in Transferable Intermolecular Potential Four Point Fluctuating Charge Water: An Assessment of Simulation Methodology and Force Field Performance and Transferability. *J. Chem. Phys.* **2007**, *127*, 064509–19.

(13) Hünenberger, P.; Reif, M. In *Single-ion Solvation - experimental and theoretical approaches to elusive thermodynamic quantities*; Hirst, J., Jordan, K., Lim, C., Thiel, W., Eds.; RSC Theoretical and Computational Chemistry Series; RSC, 2011.

(14) Northrup, S. H.; Hynes, J. T. The stable states picture of chemical reactions. I. Formulation for rate constants and initial condition effects. *J. Chem. Phys.* **1980**, *73*, 2700–2714.

(15) Joung, I. S.; Cheatham, I., Thomas E. Molecular Dynamics Simulations of the Dynamic and Energetic Properties of Alkali and Halide Ions Using Water-Model-Specific Ion Parameters. *J. Phys. Chem. B* **2009**, *113*, 13279–13290.

(16) Tielrooij, K. J.; van der Post, S. T.; Hunger, J.; Bonn, M.; Bakker, H. J. Anisotropic Water Reorientation Around Ions. *J. Phys. Chem. B* **2011**, *115*, 12638–12647.

(17) van der Post, S. T.; Bakker, H. J. The Combined Effect of Cations and Anions on the Dynamics of Water. *PCCP* **2012**, *14*, 6280–6288.